RSCPublishing   Faraday Discussions

Photoelectron-photofragment coincidence studies of I_3^- using an electrospray ionization source and a linear accelerator

SCHOLARONE™
Manuscripts

Photoelectron-photofragment coincidence studies of I_3^- using an electrospray ionization source and a linear accelerator

J. A. Gibbard[a] and R. E. Continetti[a]

Photoelectron-photofragment coincidence (PPC) spectroscopy is used to examine the dissociative photodetachment (DPD) of I_3^-. The high beam energy PPC spectrometer for complex anions couples an electrospray ionization source, an hexapole accumulation ion trap and a linear accelerator to produce fast beams of I_3^- ($M = 381$ amu) anions, the heaviest system studied to date. Following photodetachment, the photoelectron and up to three photofragments are recorded in coincidence yielding a kinematically complete picture of the DPD dynamics at beam energies of 11 keV and 21 keV. Photodetachment leads to the production of stable I_3, two-body DPD, as well as evidence for two- and three-body photodissociation. DPD is found to occur predominantly via the first excited A state, with some contributions from highly excited vibrational levels in the neutral ground state. With the ions thermalized to 298K in the hexapole trap, there are significant contributions from vibrational hot bands. Three-body photodissociation at 4.66 eV is found to occur preferentially via a charge-symmetric process to form $I + I^- + I$. In the future this method will be applied to other polyatomic systems with a large molecular mass, including multiply charged anions and complex clusters, in concert with a cryogenically cooled hexapole trap to reduce thermal effects.

1 Introduction

The photodissociation dynamics of the triiodide anion I_3^- and triiodine radical I_3 have been studied in the gas phase,[1–8] motivated by the fundamental role played by these species in a wide range of chemical processes. The rate of recombination of $2I \longrightarrow I_2$ following photodissociation of I_2, is significantly enhanced when the third body chaperone is itself I_2, and the chemically bound triiodine radical I_3 is formed as a reaction intermediate.[9–13] The accepted mechanism for this fundamental gas phase reaction is $I + I_2 \longrightarrow I_3^*$, $I_3^* + M \longrightarrow I_3 + M$, $I + I_3 \longrightarrow 2I_2$, where M is a third body. Interconversion of the nuclear spin states of I_2 is also proposed to occur via the formation of an I_3 intermediate following a three-body collision with an I atom, $I + I_2 + M \rightleftharpoons I_3 + M$, where the reverse reaction produces ortho- and para-I_2 in their statistical weights.[14]

When photodetachment of an anion yields a neutral on a repulsive potential energy surface, a photoelectron and multiple neutral fragments are formed via the process of dissociative photodetachment (DPD). Photoelectron-photofragment coincidence (PPC) spectroscopy builds on photoelectron spectroscopy, by coupling it with translational spectroscopy of the resulting neutrals, to give a kinematically complete picture of the DPD dynamics.[15] The high beam energy PPC spectrometer combines an electro-

spray ionization (ESI) source, an hexapole accumulation trap and a linear accelerator (LINAC) to study multiply charged anions, clusters and complex anions relevant to biological, atmospheric and combustion processes.[16] In this manuscript this PPC spectrometer is used to study the DPD and photodissociation dynamics of I_3^-, the heaviest system studied to date.

The triiodide anion, I_3^- has been extensively studied in the gas, liquid and solid phase using optical absorption, resonance Raman and magnetic circular dichroism spectroscopy.[17–24] The condensed phase absorption spectra and gas phase photofragment yield spectra of I_3^- are dominated by two broad features centered at 290 nm and 360 nm, known as the C and D band in solution.[2,25] However, product branching ratios differ between the gas and the condensed phase.[26] The accepted assignment for these two features is excitation from the ground $X\ {}^1\Sigma_g^+$ state to the excited states ${}^3\Pi_{0^+u}$ and ${}^1\Sigma_{0^+u}$ respectively.[2,19,25,27] Below 280 nm in the gas phase a sharp drop in photofragment yield is seen as photodetachment becomes a competitive process to photodissociation.[2,25] I_3^- has been used as a test system for studying photodissociation dynamics in solvation.[2–8,28–30] Ruhman and coworkers have studied the photodissociation of $I_3^- \longrightarrow I + I_2^-$ in alcohol solutions and observed coherent vibrational excitation of the resulting diiodide anions.[5–8,29,30]

Femtosecond photoelectron spectroscopy,[26] translational spectroscopy[2,3] and photofragment mass spectroscopy[25,31] have been used to study the photodissociation of I_3^-. The emergence of I^-

[a] Department of Chemistry and Biochemistry, University of California, San Diego, 9500 Gilman Dr, La Jolla, Ca, 92093-0340, USA. E-mail rcontinetti@ucsd.edu

and I_2^- photoproducts was shown to occur within 300 fs by femtosecond photoelectron spectroscopy.[26] The I_2^- products were formed in a highly vibrationally excited state, and exhibited coherent oscillations similar to those seen in solution.[26] Translational spectroscopy at photon energies of $2.95 - 5.16$ eV demonstrated the presence of multiple dissociation pathways by reporting the kinetic energy release (KER) spectrum of the neutral fragments produced during photodissociation, either directly or by subsequent photodetachment of the ionic products.[2,3] At photon energies ≤ 3.87 eV, vibrationally excited $I_2^-(X\ ^2\Sigma_u^+) + I(^2P_{3/2})$ and $I^-(^1S) + I_2(A\ ^3\Pi_{1u})$ are the dominant two-body channels, whereas above 3.87 eV, $I(^2P_{1/2}) + I_2^-(X\ ^2\Sigma_u^+)$ dominates. At all wavelengths, apart from the lowest photon energy, the three-body channel $I(^2P_{3/2}) + I(^2P_{3/2}) + I^-(^1S)$ dominates over the two-body channels, and is believed to proceed via a synchronous concerted decay mechanism. Evidence for the $I(^2P_{3/2}) + I(^2P_{1/2}) + I^-(^1S)$ channel is seen in the translational energy spectra reported for excitation at 4.15 eV and 4.28 eV, the highest photon energies reported.[3] In the photofragment mass spectrometry study the mass spectrum of ionic products was measured as a function of wavelength, yielding a measure of the branching ratios for the production of I^- and I_2^-.[25,31] Both ionic fragments were formed across the range of excitation energies studied, implying the competitive occurrence of a range of photodissociation products, both two- and three-body channels yielding I^- and two-body channels yielding I_2^-, suggesting nonadiabatic dynamics on the excited state repulsive surfaces. A more recent study used photofragment time of flight mass spectrometry to measure the kinetic energy and angular distributions of the photofragment ions and photoneutrals between the energy of $3.36 - 4.27$ eV.[31] Across this energy range it was found that three-body photodissociation proceeds via a charge-asymmetric process i.e. the charge is located on one of the I atoms at the ends of the I_3^- anion, rather than the central atom, to $I(^2P_{3/2}) + I(^2P_{3/2}) + I^-(^1S)$ products. No evidence was seen for the $(^2P_{3/2}) + I(^2P_{1/2}) + I^-(^1S)$ channel which is energetically accessible at the highest photon energies used. At photon energies within the 360 nm absorption band of I_3^- the dominant two-body channels were seen to be $I^-(^1S) + I_2(X\ ^1\Sigma_g^+)$ or $I^-(^1S) + I_2(A\ ^3\Pi_{1u})$ and a smaller contribution from $I\ (^2P_{3/2}) + I_2^-(X\ ^2\Sigma_u^+)$, whereas at 4.27 eV $I(^2P_{1/2}) + I_2^-(X\ ^2\Sigma_u^+)$ dominated with a small contribution from $I^-(^1S) + I_2(B\ ^3\Pi_{0u}^+)$. The branching ratios seen by Nagata and coworkers differ from those measured by Neumark and coworkers. A preference for formation of I^- rather than I_2^- and two-body rather than three-body processes was seen in the photofragment mass spectrometry studies. Ab initio calculations presented suggested that the potential energy surface of the I_3^- is complex, and characterized by numerous conical intersections and avoided crossings,[31] which is consistent with the ab initio and diatomics-in-molecules calculations of Harvey and coworkers.[25,32]

The triiodine radical was first isolated using high resolution photoelectron spectroscopy by Neumark and coworkers, almost twenty years ago, and since then numerous excited states of the radical have been characterized.[1,22] The electron affinity $(4.226 \pm 0.013$ eV)[22] and the vertical detachment energies of the excited X, A, B and C states of I_3 have been determined by pho-

toelectron spectroscopy.[1,22] A vibrational progression has been recorded for the ground X state, yielding a vibrational frequency of $v_0 = 115$ cm^{-1}, assigned to the symmetric stretch of I_3. The symmetric stretch of the anion has a harmonic frequency of $v_0 = 112$ cm^{-1}.[26] This extended vibrational progression has been attributed to poor Franck-Condon overlap between the vibrational ground states of the anion and the neutral, due to the significant change in the equilibrium bond length.[22] The experimentally determined anion bond length in the solid state is 2.93 Å[33] and calculations predict the neutral bond length to be between 2.76 Å and 2.84 Å.[32,34] No vibrational structure was recorded for the excited neutral states.

The photodissociation dynamics of the triiodine radical have also been studied by Neumark and coworkers in the gas phase using translational spectroscopy.[1] Photodetachment of I_3^- with a nanosecond laser was used to produce a beam of the ground state radical $I_3(X)$. These radicals were subsequently photodissociated by a second nanosecond laser pulse. In those experiments, two- and three-body photodissociation channels were accessible, with $I_2 + I$ and $I + I + I$ products formed in the ground and excited sates electronic states accessible at photon energies of $4.59 - 5.17$ eV.[1] Channels with excited state products dominated, and significant rotational and vibrational excitation was seen in the products regardless of electronic state. Branching ratios were not accurately determined due to the rovibrational excitation in the products, but channels with only ground electronic state products seemed unfavorable.

The ground states of the anion and the radical have linear, centrosymmetric structures.[22,35–39] Triiodide is a well-known example of a hypervalent 22 electron molecule that violates the octet rule,[35–37] and is one of the few closed shell anions with excited electronic states below the electron detachment threshold.[17] Triiodine is the most stable trihalogen radical.[38,39] The ground state closed-shell electron configuration of I_3^- is $X\ ^1\Sigma_g^+$ $\sigma_u^2\ \pi_u^4\ \pi_g^4\ \sigma_g^2\ \pi_u^{*4}$.[18,27] The ground state electron configuration of I_3 can be approximated by removing an electron from the highest occupied molecular orbital of I_3^- in accordance with Koopman's theorem,[18,27] yielding $\sigma_u^2\ \pi_u^4\ \pi_g^4\ \sigma_g^2\ \pi_u^{*3}$. This electron configuration is split by spin-orbit coupling to predict a $^2\Pi_{u,3/2}$ ground state, and a $^2\Pi_{u,1/2}$ first excited state. Pyykkö and coworkers predicted that the $\sigma_u^2\ \pi_u^4\ \pi_g^4\ \sigma_g^1\ \pi_u^{*4}$ electron configuration would yield a $^2\Sigma_g^+$ state lower in energy than the $^2\Pi_{u,1/2}$ state due to the large spin-orbit coupling of I using an extended Hückel model.[40] The relative ordering of these three radical states has been the focus of some discussion.

Coker and coworkers have modeled the ground and excited state potential energy surfaces of the I_3 radical using a semi-empirical diatomics-in-molecules approach.[34,41,42] This model assumes a linear structure for I_3 and treats it in accordance with Hund's case C. The $\Omega = 1/2$ ground state, where Ω is the projection of the total angular momentum onto the molecular axis, was found to be symmetric and weakly bound by 0.19 eV relative to the $I + I_2$ dissociation asymptote. The $\Omega = 3/2$ first excited state is also predicted to be weakly bound with a linear equilibrium geometry along the symmetric stretch coordinate, however the surface has two wells either side of the linear geometry, correspond-
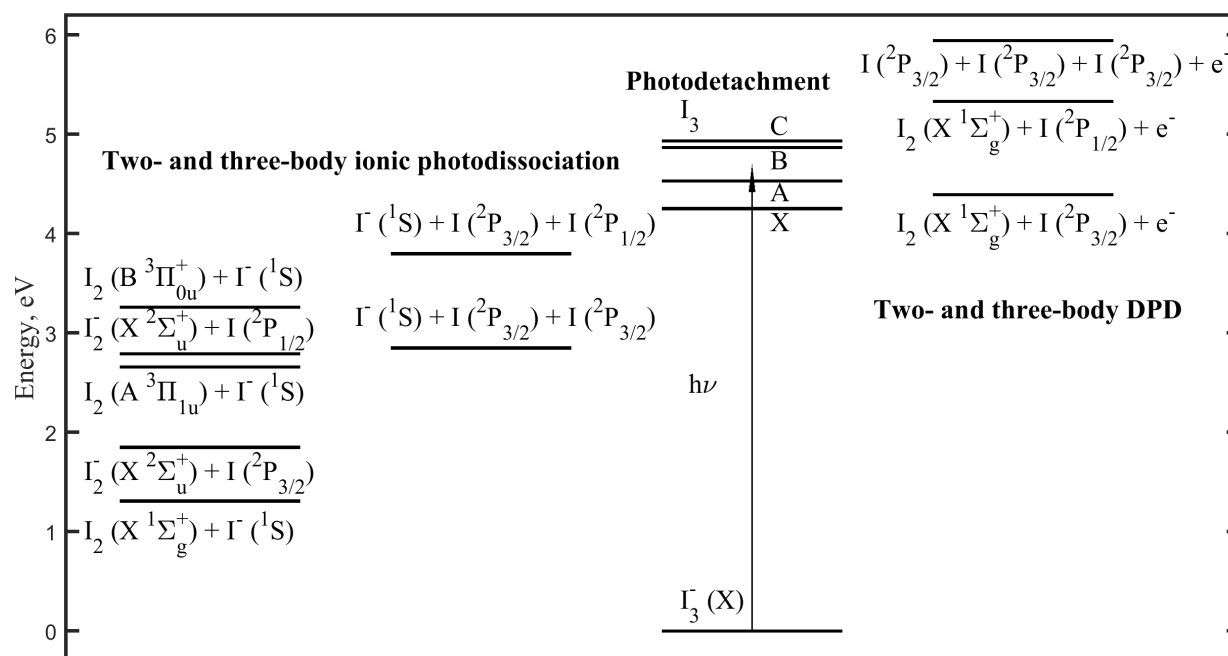
Fig. 1 The potential energy diagram of I_3 and I_3^- including the excited neutral states. [1,22] Asymptotes for two- and three-body DPD and ionic photodissociation channels are also shown. [1-3] The 266 nm photon energy is shown as $h\nu$.

ing to asymmetric geometries, leading to dissociative character on the potential energy surface. The $\Omega = 3/2$ second excited state has a deep well and a linear equilibrium geometry. The approach has successfully reproduced the photoelectron spectra measured by Neumark and coworkers, [26] including the ground state vibrational progression. It seems likely that the $\Omega = 1/2$ ground state from Coker and coworkers is the $^2\Sigma_g^+$, and the $\Omega = 3/2$ first excited state the $^2\Pi_{u,3/2}$, corresponding to the X and A state measured in the photoelectron spectra. However, high level *ab initio* calculations on the electronic structure of I_3 for a variety of point groups have been carried out by Harvey and coworkers, that assign the ground state to the $^2\Pi_{u,3/2}$ state. [32] In the absence of spin-orbit coupling I_3 is predicted to be bent with a bond angle of 145.4° similar to the Br_3 radical where Renner-Teller coupling splits the $^2\Pi_u$ state into $^2A_1$ and $^2B_1$ states. However, spin-orbit coupling stabilizes the linear geometries more than the bent resulting in a linear, centrosymmetric ground state for I_3. Similarly, the ground states of Cl_3 and Br_3 are both $^2\Pi_{u,3/2}$. [43] The electron affinity is calculated to be 4.025 eV (experimental value 4.226 eV), [22] but the spacing between the ground and excited state are in excellent agreement with experiment. [32]

Fig. 1 shows the energy level diagram for I_3, I_3^- and the ionic photodissociation and DPD product channels, using values reported in the photoelectron and translational spectroscopy studies of Neumark and coworkers. [1-3,22] Assuming the anion is in its ground vibrational state, the X and A neutral states are accessible with a 266 nm photon. Only one DPD asymptote is energetically accessible at this photon energy, a two-body $I_2 + I + e^-$ channel, where both the atom and the diatomic are formed in the ground electronic state. Other two- and three-body DPD channels are out of range, with the lowest lying $I + I + I$ channel 1.3 eV above the

photon energy. In the experiments described in this manuscript the neutral states are accessed directly from the anion ground state via a one-photon process, rather than a two-photon process of photodissociation following photodetachment used in previous studies. There are a multitude of accessible two- and three-body photodissociation channels. I_3 is bound with respect to dissociation by 0.143 eV, whereas the A state lies 0.279 eV above the X state, or 0.136 eV above the lowest dissociation asymptote. Here PPC spectroscopy is used to extend these previous photodissociation studies to include direct studies of DPD processes.

2 Experimental

The experiments were carried out on the high beam energy PPC spectrometer shown in Fig. 2. The apparatus has been described in detail elsewhere. [16] Gas phase I_3^- was produced using ESI of a 2.5 mmol solution of KI(s) and I_2(s) in methanol. Previous studies have produced I_3^- by flowing Ar gas over I_2 crystals, before supersonically expanding the beam and intersecting it with an 1 kV electron beam. [1,22] ESI provides an easy and efficient alternative method to produce I_3^-. Anions are desolvated in a heated capillary, and pass through a differentially pumped skimmer, before passing into an octopole ion guide to efficiently transfer anions into the ion trap. The anions are thermalized to 298K via collisions with room temperature He buffer gas in a hexapole accumulation ion trap. The anions are trapped via a radiofrequency field (RF) field, [44] and two endcaps are switched initially to trap the anions, and then eject short, intense pulses of room temperature anions. Acceleration to anion beam energies in the tens of keV occurs in a 10-stage linear accelerator (LINAC). [45] The beam energy can be tuned by adjusting the acceleration potential on the LINAC, and the timed elements of the acceleration stages results
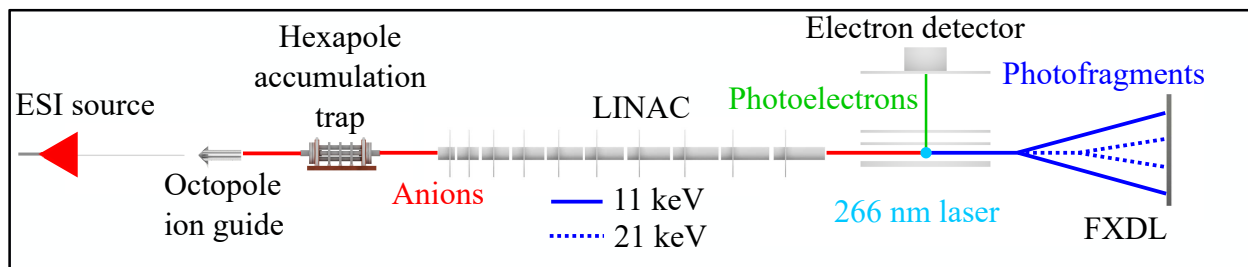
Fig. 2 Schematic of high beam energy PPC spectrometer. Anions are produced via ESI on the left hand side, cooled in the hexapole accumulation trap, accelerated by the LINAC before interaction with the laser to induce photodetachment, photodissociation and DPD. The photoelectron and up to three photofragments are recorded in coincidence in the PPC detector on the right hand side. The effect of beam energy on the dissociating neutral fragments is depicted.

in a very narrow m/z being transmitted to the detector. The LINAC increases the range of masses which can be studied using PPC, by increasing the acceleration potential which can be applied to the ions.[16] The fast anion packet is focused into the detector region via a series of deflectors, einzel lens, a compressor[46] and a Bakker mass spectrometer.[47]

The 4th harmonic of a mode-locked, Q-switched, cavity-dumped Nd:YAG is used to photodetach the anions.[48] The ejected photoelectrons are extracted perpendicular to the ion beam, and imaged on a time and position sensitive microchannel plate (MCP) detector. An image of the photoelectron x, y positions encoding the electron kinetic energy (eKE), and the photoelectron angular distribution is produced. Additionally, the flight time of the electron from the interaction region to the detector is recorded. The resulting neutral photofragments, whether stable I_3 or the products of dissociation, strike the neutral detector (FXDL) which can record the position and arrival time of up to three fragments.[49] Using the conservation of energy and momentum the KER of any pairs or triples of dissociating fragments originating from the same anion can be calculated. In Fig. 2 the trajectories for the neutral fragments resulting from anions at beam energies of 11 keV and 21 keV are indicated. Higher beam energies result in a smaller dissociative neutral spot on the FXDL, and a narrower range of arrival time for fragments at the FXDL than for slower parent anions.[50] Additionally the higher detection efficiency of high beam energy measurements results in faster data acquisition times and better discrimination against false coincidences. Undetached anions are deflected out of the neutral beam path, and onto a MCP detector to monitor the ion signal in real time.

3 Results

I_3^- was studied by PPC spectroscopy at beam energies of 11 keV and 21 keV. Photoelectron images and eKE spectra, KER spectra, and $E_{TOT} = eKE + KER$ spectra were measured. PPC measurements record the eKE for a dissociative event in coincidence with the KER, and the resulting correlation can be plotted in a 2D histogram of N(eKE, KER) known as a PPC spectrum.[15] Photodetachment of I_3^- was found to yield stable I_3, the two-body DPD products of $I_2 + I + e^-$ and the products of multiple ionic photodissociation channels. The two-body DPD channel and the

photodissociation channels[1,2] will be discussed in turn.

The data from the PPC measurements of I_3^- at both beam energies was very similar, and the same conclusions can be drawn from the data. Most of the data presented in this manuscript was recorded at 21 keV, as high beam energy measurements result in neutral fragments with a larger detection efficiency, which in turn results in better discrimination against false coincidences. The faster data acquisition rates associated with higher beam energies is especially significant for three-body channels, where the probability of detecting all three fragments and the electron in coincidence is very low. The only 11 keV I_3^- results shown are the time of flight spectra where the slower parent anions result in better separation of peaks in the time of flight spectrum.

3.1 Two-body DPD

Fig. 3 shows the total, two-body dissociative, and stable photoelectron spectra of 21 keV I_3^- at 266 nm. The total photoelectron spectrum contains all of the photoelectrons recorded in coincidence with at least one fragment, and has contributions from one-, two- and three-body processes. The measured eKE of the ground X state and first excited A state are consistent with those previously recorded by Neumark and coworkers.[1,22] Each spectra is normalized to the maximum intensity of the A state. The width of the features in Fig. 3 indicates the I_3^- anions produced via ESI and thermalized to room temperature in an ion trap, have more internal excitation than the I_3^- anions produced via a supersonic expansion in the Neumark study. Some of the width in the X state is expected to come from the extended vibrational progression previously reported in the photoelectron spectra of the I_3^- anion, seen due to the large change in equilibrium bond length between the anion and the radical ground states.[22] The inset of Fig. 3 is a photoelectron image of the total photoelectron spectra. The outer ring is the ground $^2P_{3/2}$ state of I, indicating the presence of a photodissociation channel forming I^-, and then subsequent photodetachment via a two-photon process. The channel is present in the eKE data but of very low intensity.

The stable photoelectrons were recorded in coincidence with a single stable neutral product i.e. a neutral I_3, and gated in position and time to reduce the contribution from two-body events distributed across the detector face where only a single fragment is measured. The photodetachment events yielding stable I_3 form
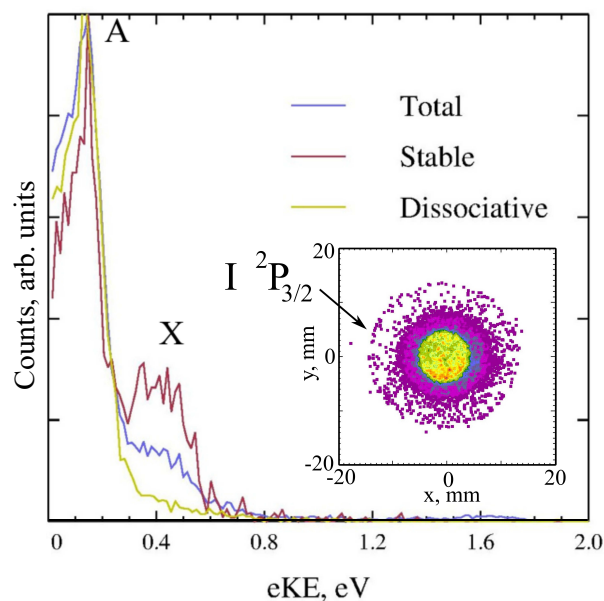
Fig. 3 Photoelectron spectra of 21 keV I_3^- gated for two-body dissociative events, one-body stable events and total events. Each spectra is normalized to the maximum intensity of the A state. Photoelectrons are recorded in coincidence with at least one neutral fragment. The inset shows the total spectra plotted as a photoelectron image to clarify the outer ring corresponding to the photodetachment of I^- (^1S) to $I(^2P_{3/2})$.

Fig. 4 KER spectra of two-body DPD resulting in $I+I_2$ at 11 keV and 21 keV

a small feature at the center of the FXDL, which can be spatially resolved from the broad feature on the FXDL formed via dissociative fragments.[50] In this case a stable fragment is one which does not dissociate on the timescale of the flight between the interaction region and the FXDL.

The dissociative photoelectrons were recorded in coincidence with a pair of neutral fragments, in this case the products of two-body DPD, $I_2 + I$ as discussed later. Here the data is gated to select for the broad dissociative feature on the FXDL, so multiple events that occur during the same laser shot and result in multiple stable I_3 fragments are not included. The photoelectron spectra gated for one- or two-body events have significantly different intensities in the A and X states, with the stable photoelectrons having more intensity in the neutral ground X state, and dissociation occurring predominantly from the A state. From Fig. 1 the A state lies above the $I+I_2+e^-$ dissociation asymptote, whereas the X state is stable with respect to dissociation.

When a neutral dissociates the fragments recoil from the parent anion trajectory conserving energy and angular momentum. The kinematics of the dissociation allow determination of the number and mass of the fragments. Fig. 4 plots the two-body KER spectrum for 11 and 21 keV I_3^- at 266 nm. As shown in Fig. 2 the higher beam energy results in a dissociative feature with a smaller radius than the same dissociative feature recorded at a lower beam energy. This is because the lab frame velocity of the fragments is the sum of the recoil velocity and beam energy dependent center-of-mass velocity. The KER spectra are dependent only on the recoil velocity of the fragments. The fragments included in the KER spectra arrived as a pair of neutral fragments in coincidence with an electron, indicating a two-body dissociation,
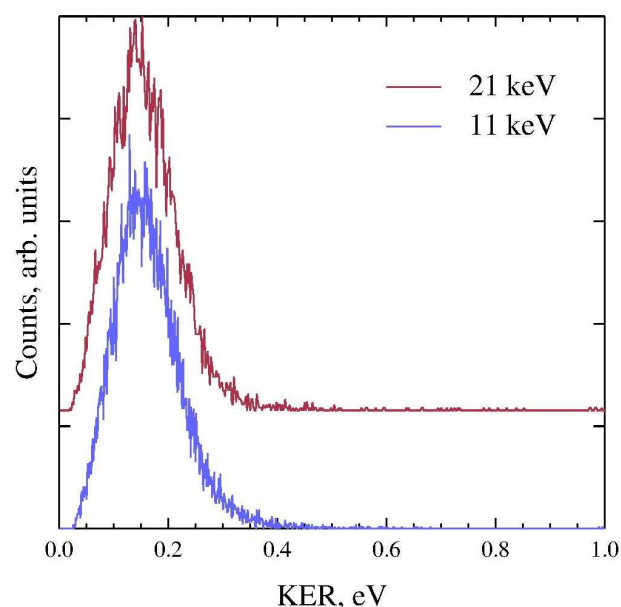
as confirmed by analyzing the arrival times of the fragments. The fragment mass can also be calculated from the arrival times and position data indicating a 2:1 mass ratio. In this triatomic system this can only mean formation of $I+I_2$. There is a single relatively sharp feature in the KER spectra peaking at 0.15 eV. This feature requires careful gating as the low KER means there is significant overlap with the stable I_3 on the FXDL which is difficult to spatially resolve. The KER spectra are gated in the same way as the dissociative photoelectrons in Fig. 3. The KER at the two different beam energies of 11 keV and 21 keV are very similar indicating that dissociation is prompt on the timescale of the flight time between the interaction region and the FXDL. Two-body DPD from the A state to the ground state $I+I_2$ asymptote would be expected to yield a KER of 0.14 eV, strongly indicating that this KER is a result of DPD to $I+I_2+e^-$ via the A state of the I_3 neutral. The lack of vibrational structure indicates that the A state has repulsive character and leads to dissociation on a timescale smaller than the vibrational period of the I_3. This plus the observed feature in the photoelectron spectra indicate that the A state potential energy surface is similar to the first excited state of I_3 calculated by Coker and coworkers, which is bound along the symmetric stretch coordinate, but dissociative in character for asymmetric geometries leading to the lowest lying $I+I_2+e^-$ products.

Fig. 5 shows the two-body PPC spectrum for I_3^-. There is one feature of almost Gaussian intensity centered at KER= 0.15 eV, and eKE= 0.15 eV. This indicates two-body DPD from the A state of the neutral to the lowest dissociation asymptote of $I+I_2+e^-$. The maximum kinetic energy of all the fragments, KE_{max}, assuming two-body DPD to the $I_2 + I + e^-$ channel can be calculated from the photon energy, the electron affinity of the neutral and
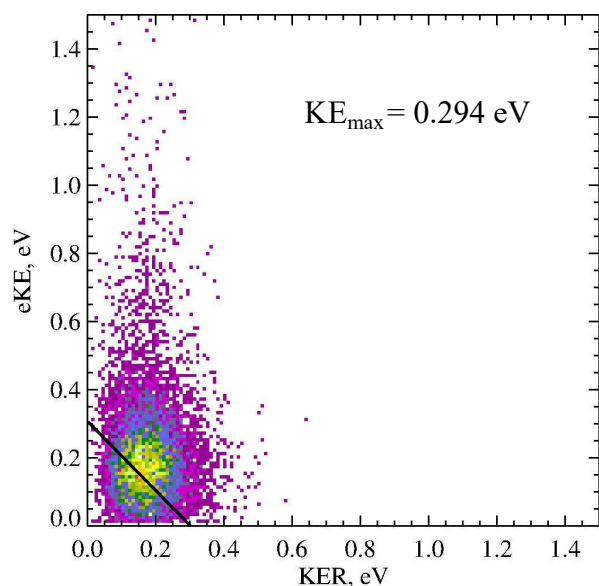
Fig. 5 Two-body PPC spectra of $21\,\text{keV}$ I_3^- showing two-body DPD. The black line indicates the $KE_{max} = 0.294\,\text{eV}$ calculated from the potential energy diagram in Fig. 1.
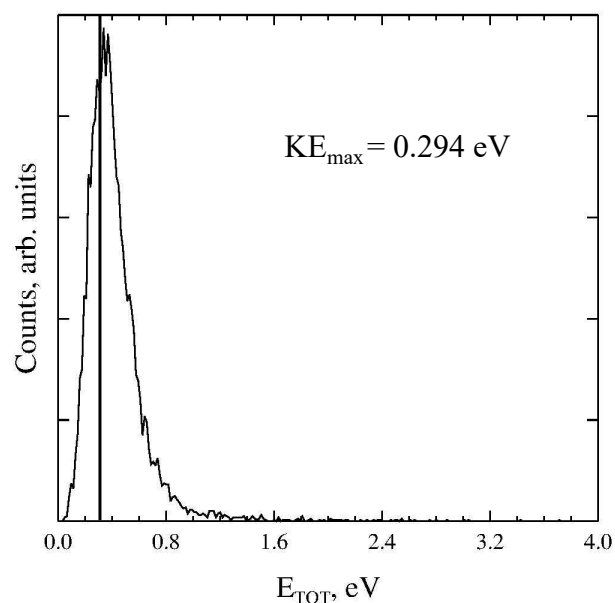
Fig. 6 The E_{TOT} spectrum for two-body events recorded in coincidence with a photoelectron for $21\,\text{keV}$ I_3^-. The black line indicates the $KE_{max} = 0.294\,\text{eV}$ calculated from the potential energy diagram in Fig. 1.

the binding energy of the neutral,[1,22]

$$KE_{max} = \lambda(1) - EA(I_3) - D_0(I + I_2)$$

$$= 4.66\,\text{eV} - 4.226\,\text{eV} - 0.14\,\text{eV} \qquad (1)$$

$$= 0.294\,\text{eV}$$

The calculated value is plotted in black in Fig. 5, and matches well with the experimental maximum indicating two-body DPD. The feature extends beyond the theoretical KE_{max} indicating the parent anion has significant internal excitation. The extension of the feature to larger eKE values may indicate the presence of dissociation products from vibrationally excited ground state I_3.

Fig. 6 plots the total kinetic energy, $E_{TOT} = eKE + KER$, for the dissociative events recorded at $21\,\text{keV}$ I_3^-. The peak of the distribution is $0.3\,\text{eV}$, which matches well with the calculated KE_{max}, plotted as the black line in Fig. 6. Events that occur to the high energy side of this line indicate excited anions, which results in an increase in the E_{TOT} available to partition between the fragments following photodetachment. However the energy resolution of the measurement of E_{TOT} is dependent on the energy resolutions of the eKE and the KER, which are typically 5%[16] and 10%,[51] yielding an energy resolution for E_{TOT} of 11%. This significant uncertainty is more likely to broaden the distribution than shift the peak position, hence E_{TOT} is considered to be in good agreement with the calculated KE_{max}. The high energy tail with low intensity can be attributed to the high energy tail in the dissociative photoelectron spectra in Fig. 3. Similar features in the calibration photoelectron spectrum of I^- indicate that it is not representative of the anion vibrational temperature, but characteristic of the apparatus. One source of this high energy tail is the electron resolution which is dominated by uncertainty in the electron velocity component perpendicular to the plane of the electron detector v_z.[52] It

is possible to minimize this effect by slicing the eKE spectrum in time, but it is always present as the electron detector is optimized for velocity map imaging of the photoelectrons.[53] Additionally false coincidences between neutral fragments and spurious electrons produced when the UV laser noise interacts with metallic surfaces in the experiment, contribute to the tail. Previous measurements on I_2^- indicated that the anions have significant rovibrational excitation consistent with a vibrational temperature of 298K.[16] The anion temperature is largely due to thermalization with the room temperature buffer gas in the hexapole accumulation trap. In the future the hexapole accumulation trap will be cryogenically cooled, reducing the anion vibrational temperature to $\approx 10\text{K}$.

3.2 Photodissociation

Photodissociation cannot be studied directly using PPC spectroscopy, unless photodissociation is followed by photodetachment or autodetachment of the resulting anionic product. In these cases, photoelectrons and neutral fragments are the only products that can be recorded in a kinematically complete measurement by PPC spectroscopy. Excluding autodetachment, this only occurs via a two-photon process and is therefore dependent on the laser fluence. In our experiments the low laser power makes the probability of photodetachment following photodissociation low. Therefore, a two-body photodissociation is more likely to yield a single neutral fragment than a pair of fragments and a photoelectron, and three-body photodissociation is more likely to produce a pair of neutral fragments than three fragments and a photoelectron. In the current study, at $4.66\,\text{eV}$, stable I_3 and the products of DPD dominate, but some small signal is seen which can be attributed to photodissociation. As described earlier both Nagata and coworkers, and Neumark and coworkers have
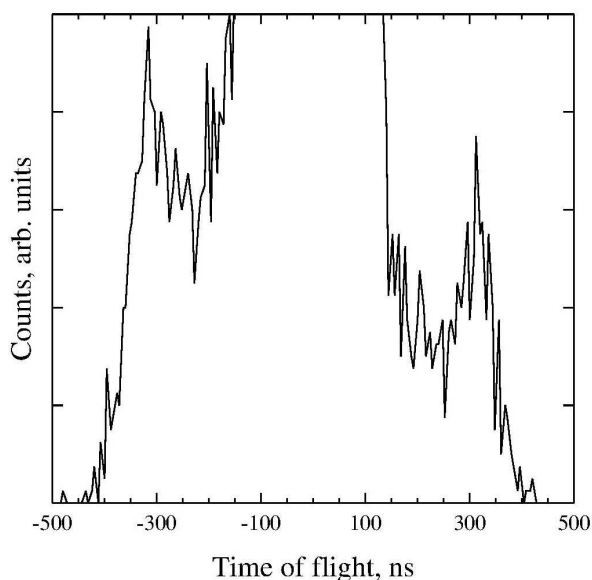
Fig. 7 Time of flight spectrum for single neutral fragments produced via photodetachment of $21\,\text{keV}\ I_3^-$ at 266 nm. High intensity feature centered at $t = 0$ ns is from stable I_3, whereas the early or late fragments result from dissociation when only a single fragment is recorded, providing evidence for two-body photodissociation.
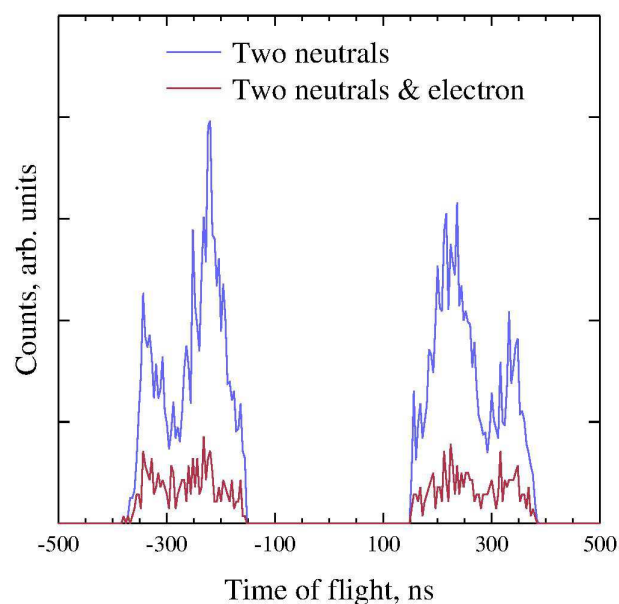
Fig. 8 Time of flight spectrum for two-body events which arrive in co-incidence with a photoelectron and without. Fragments resulting from two-body DPD would arrive between $-100\ \text{ns} < t < 100\ \text{ns}$ and have been gated out of the figure.

performed studies into the photodissociation of I_3^-.[2,3,25,26,31] No KER spectra for the photodissociation products of I_3^- above the electron affinity of I_3 have previously been reported.
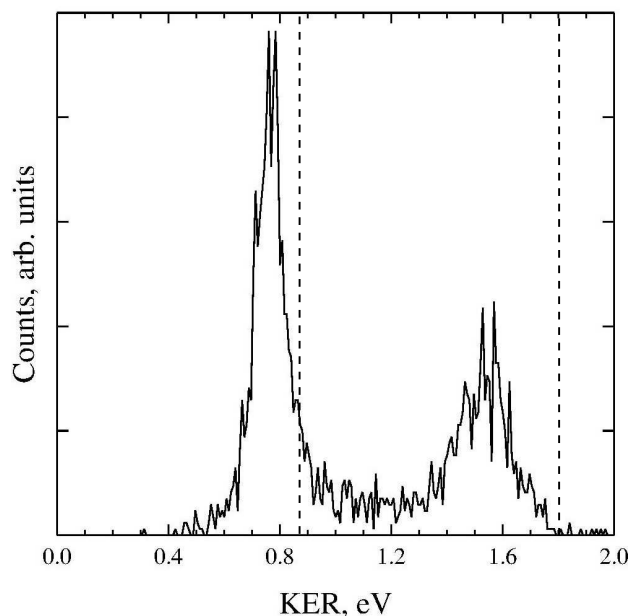
3.2.1 Two-body photodissociation

Multiple two-body photodissociation channels are energetically accessible at the photon energy of 4.66 eV leading to the products; $I^-\,(^1S) + I_2(X\ ^1\Sigma_g^+)$, $I(^2P_{3/2}) + I_2^-(X\ ^2\Sigma_u^+)$, $I^-\,(^1S) + I_2(A\ ^3\Pi_{1u})$, $I(^2P_{1/2}) + I_2^-(X\ ^2\Sigma_u^+)$ and $I^-\,(^1S) + I_2(B\ ^3\Pi_{0u}^+)$ in ascending energetic order.[3] Previous studies have reported that the fourth channel ($I(^2P_{1/2}) + I_2^-(X\ ^2\Sigma_u^+)$) is the dominant two-body photodissociation channel at 4.27 eV, with a minor contribution from the fifth channel ($I^-\,(^1S) + I_2(B\ ^3\Pi_{0u}^+)$), producing both I^- and I_2^-.[3,31] A single feature arising from two-body DPD is seen in the two-body PPC spectra shown in Fig. 5, indicating that any two-body photodissociation followed by photodetachment has a negligible rate. Furthermore, no features in the dissociative photoelectron spectrum in Fig. 3 can be attributed to photodetachment of either I^- or I_2^-. The atomic anion would yield sharp features and the photoelectron spectra of the diatomic anion extends to significantly higher eKE. Therefore, the only detectable product of two-body photodissociation is a single neutral fragment.

Fig. 7 shows the time of flight spectrum for a single fragment centered at the arrival time for stable I_3. The intense feature at t=0 is the stable I_3 and is not discussed in this section. Wings in the spectrum indicate the presence of fragments forward and backward scattered along the ion beam propagation direction, but not correlated with a second fragment. The early and late arrival times indicate these fragments are formed via a dissociative process with a significant KER, resulting in fragments which are recoiling from the center-of-mass velocity. The arrival times of the fragments do not overlap with the arrival times for fragments

produced via two-body DPD, indicating a two-body photodissociation process. The low intensity of these features at early or late arrival time indicates that these two-body photodissociation channels are minor channels at this photon energy. In total, the limited information that can be extracted from this single neutral fragment data indicate the presence of at least one two-body photodissociation channel.

3.3 Three-body photodissociation

The three-body DPD to $I+I+I+e^-$ is expected to be out of range at the current photon energy, but three-body photodissociation to $I^-\,(^1S) + I(^2P_{3/2}) + I(^2P_{3/2})$ has been the dominant three-body photodissociation channel seen in previous studies at all wavelengths when it is energetically accessible, and has been found to be promoted by vibrational excitation.[3] Three-body photodissociation to $I^-\,(^1S) + I(^2P_{3/2}) + I(^2P_{1/2})$ is also energetically accessible at the photon energy used here, but Nagata and coworkers saw no evidence for it,[31] and Neumark and coworkers saw it only as a minor channel at the highest photon energies.[3] In these experiments only neutral fragments are detected, so the one-photon products of three-body photodissociation are two neutral fragments recorded without an electron in coincidence. Fig. 8 shows the arrival times for pairs of neutrals recorded with and without an electron in coincidence, where the two-body DPD signal has been gated out. The signal is far larger for the two neutral events without an electron in coincidence, implying that these neutrals produced with ionic fragments, rather than a photoelectron. The inner peaks correspond to a pair of fragments arriving at the FXDL in coincidence, and the outer peaks form a second pair. In total this implies two separate three-body photodissociation channels, yielding $I+I+I^-$ in various electronic states.

Fig. 9 KER spectrum for I+I resulting from three-body photodissociation of 21keV I_3^-. The gating is the same as Fig. 8. The dashed black lines indicate the calculated KER for the $I(^2P_{3/2}) + I(^2P_{3/2}) + I^-(^1S)$ and $I(^2P_{3/2}) + I(^2P_{1/2}) + I^-(^1S)$ channels.

In the case of photodissociation, any excess energy after the bond is broken is transferred into the KER of the products, or internal excitation of any molecular product fragments. Useful energetics can be gained from measurement of only the two neutral products here as the fragments are atoms and all the excess energy is appears as the KER. For a three-body dissociation the KER is,

$$\mathrm{KER} = \frac{1}{2}m_1 V_1^2 + \frac{1}{2}m_2 V_2^2 + \frac{1}{2}m_3 V_3^2 \qquad (2)$$

where m_1, m_2 and m_3 are the masses and V_1, V_2 and V_3 are the recoil velocities of the photofragments in the center-of-mass frame. When a linear homonuclear triatomic molecule dissociates the terminal atoms recoil with equal and opposite momentum, leaving the central atom stationary in the center-of-mass frame, such that $V_1 = -V_3$, $V_2 = 0$ and $m = m_1, m_2, m_3$. Here the recoil can be characterized by a single velocity vector $|v| = |V_1 + V_3|$. This simplifies equation 2 to KER$= \frac{1}{2}\mu v^2$, which is the equation for the KER of a two-body dissociation, as used to calculate Fig. 9. A similar approach has previously been employed in this laboratory to study O_6^-.[54] Fig. 1 shows there are two three-body photodissociation channels below the ionization threshold of I_3^-, which are energetically accessible with a 4.66 eV photon, $I(^2P_{3/2}) + I(^2P_{3/2}) + I^-(^1S)$ at $D_0 = 2.85$ eV and $I(^2P_{3/2}) + I(^2P_{1/2}) + I^-(^1S)$ at $D_0 = 3.8$ eV. These channels would be associated with a KER of 1.81 eV and 0.86 eV. Fig. 9 plots the KER for the two neutral fragments shown in Fig. 8. There are two clear features peaking at 1.55 eV and 0.75 eV, close to the calculated three-body KER values, plotted in black dashes in Fig. 9, for the $I(^2P_{3/2}) + I(^2P_{3/2}) + I^-(^1S)$ and $I(^2P_{3/2}) + I(^2P_{1/2}) + I^-(^1S)$ photodissociation channels.

Neumark and coworkers have described how three-body disso-

ciation of I_3 proceeds via a concerted synchronous mechanism.[3] In the limit of a true concerted dissociation the terminal I atoms are forward and backward scattered on equal and opposite trajectories upon dissociation, carrying away all of the energy released. However, the discrepancy between the calculated KER and the spectrum indicates that at the time of dissociation the central I atom is displaced from the center-of-mass. Vibrational excitation of the asymmetric stretch or the bending mode breaks the symmetry of the anion, leading to some translational energy being partitioned to the undetected central I atom following dissociation. The discrepancy is larger for the high KER channel.

Nagata and coworkers have presented evidence for a charge-asymmetric dissociation where the electron is localized on one of the terminal I atoms in the linear anion.[31] In order for the three-body KER to be extracted from two neutral fragments, it is necessary to collect the forward and backwards scattered fragments, in this case the terminal I atoms of the linear I_3 radical. This implies that the anions undergo a charge-symmetric dissociation, i.e. the charge is located on the central I atom, and the resulting I^- is left at the center-of-mass velocity following photodissociation. The agreement between the calculated KER and the experimental KER shown in Fig. 9 provide clear evidence for the charge-symmetric three-body photodissociation of I_3^-. The charge-asymmetric process would result in a neutral fragment arriving near the center-of-mass velocity, or $t = 0$ ns in Fig. 8, and a companion fragment arriving in either the forward or backward scattered wings. These events are difficult to isolate from false coincidences as the arrival time of the central I atom would be very similar to the arrival time of a stable I_3 or fragments from the low KER two-body DPD channel. The KER for charge-asymmetric events cannot be calculated from the arrival time and position of the two neutral fragments, hence in Fig. 9 the charge-symmetric events are selectively analyzed.

More information could be extracted if following photodissociation, photodetachment of the resulting I^- occurred. However, the PPC spectra for the three-body photodissociation data calculated from two neutral fragments in coincidence with an electron (not shown) has clear vertical stripes, an indication that this spectrum is dominated by false coincidences. This is a consequence of the low event rate for the sequential two-photon process required to yield an electron in coincidence. This is confirmed by the very small amount of data (≤ 100 events) collected where three neutrals were recorded in coincidence with an electron. This is attributed to the low laser fluence used in these experiments.

From the intensity of the KER spectrum in Fig. 9 it is clear that the low KER photodissociation channel dominates. This channel results in the production of an electronically excited I atom along with a ground state I atom and dominates over the production of two ground state I atoms which has been determined to be the dominant three-body photodissociation channel at lower photon energies.[3,31] This indicates that at the higher photon energies used in the current study, repulsive potential energy surfaces which yield the excited state products are accessible. Additionally, the vibrationally excited anions produced in the room temperature ion trap may yield good Franck-Condon overlap with different portions of the potential energy surface. Within the limita-

tions of extrapolating data about a three-body photodissociation process from a pair of neutral fragments, the data dictates that at 4.66 eV three-body photodissociation preferentially proceeds via a charge-symmetric process to produce $I^-(^1S) + I(^2P_{3/2}) + I(^2P_{1/2})$.

4 Conclusions

The DPD and photodissociation of I_3^- has been studied via PPC spectroscopy at two beam energies. Two-body DPD of I_3^- resulting in ground electronic state $I_2 + I + e^-$ has been shown to proceed via the first excited A state of the I_3 radical. Measurements at 21 keV and 11 keV are consistent, showing that dissociation is prompt. There is evidence for at least one two-body photodissociation channel. At 4.66 eV two three-body photodissociation channels are observed resulting in $I + I + I^-$ in the ground electronic state, or with an excited I atom. Notably this is observed to proceed via a charge-symmetric process producing $I + I^- + I$, with the excess charge residing on the central atom.

Conflicts of interest

There are no conflicts to declare.

Acknowledgments

Notes and references

1 H. Choi, T. R. Taylor, R. T. Bise, A. A. Hoops and D. M. Neumark, *The Journal of Chemical Physics*, 2000, **113**, 8608–8614.

2 H. Choi, R. T. Bise, A. A. Hoops and D. M. Neumark, *The Journal of Chemical Physics*, 2000, **113**, 2255–2262.

3 A. A. Hoops, J. R. Gascooke, A. E. Faulhaber, K. E. Kautzman and D. M. Neumark, *The Journal of Chemical Physics*, 2004, **120**, 7901–7909.

4 A. E. Johnson and A. B. Myers, *The Journal of Chemical Physics*, 1995, **102**, 3519–3533.

5 U. Banin, A. Waldman and S. Ruhman, *The Journal of Chemical Physics*, 1992, **96**, 2416–2419.

6 U. Banin and S. Ruhman, *The Journal of Chemical Physics*, 1993, **98**, 4391–4403.

7 U. Banin and S. Ruhman, *The Journal of Chemical Physics*, 1993, **99**, 9318–9321.

8 U. Banin, R. Kosloff and S. Ruhman, *Israel Journal of Chemistry*, **33**, 141–156.

9 D. L. Bunker and N. Davidson, *Journal of the American Chemical Society*, 1958, **80**, 5090–5096.

10 R. M. Noyes and J. Zimmerman, *The Journal of Chemical Physics*, 1950, **18**, 656–658.

11 J. A. Blake and G. Burns, *The Journal of Chemical Physics*, 1971, **54**, 1480–1486.

12 G. Porter, *Discussions of the Faraday Society*, 1962, **33**, 198–204.

13 M. I. Christie, A. J. Harrison, R. G. W. Norrish and G. Porter, *Proceedings of the Royal Society of London A: Mathematical, Physical and Engineering Sciences*, 1955, **231**, 446–457.

14 V. Balykin, V. Letokhov, V. Mishin and V. Semchishen, *Chemical Physics*, 1976, **17**, 111 – 121.

15 R. E. Continetti, *International Reviews in Physical Chemistry*, 1998, **17**, 227–260.

16 J. A. Gibbard, A. J. Shin, E. Castracane and R. E. Continetti, *Review of Scientific Instruments*, 2018, **89**, 123304.

17 A. D. Awtrey and R. E. Connick, *Journal of the American Chemical Society*, 1951, **73**, 1842–1843.

18 T. Okada and J. Hata, *Molecular Physics*, 1981, **43**, 1151–1161.

19 H. Isci and W. R. Mason, *Inorganic Chemistry*, 1985, **24**, 271–274.

20 K. Kaya, N. Mikami, Y. Udagawa and M. Ito, *Chemical Physics Letters*, 1972, **16**, 151 – 153.

21 W. Kiefer and H. Bernstein, *Chemical Physics Letters*, 1972, **16**, 5 – 9.

22 T. R. Taylor, K. R. Asmis, M. T. Zanni and D. M. Neumark, *The Journal of Chemical Physics*, 1999, **110**, 7607–7609.

23 H. Forbes and D. Lynch, *Journal of Physics and Chemistry of Solids*, 1964, **25**, 621 – 627.

24 H. N. Hersh, *Phys. Rev.*, 1957, **105**, 1410–1411.

25 L. Zhu, K. Takahashi, M. Saeki, T. Tsukuda and T. Nagata, *Chemical Physics Letters*, 2001, **350**, 233 – 239.

26 M. T. Zanni, B. J. Greenblatt, A. V. Davis and D. M. Neumark, *The Journal of Chemical Physics*, 1999, **111**, 2991–3003.

27 A. S. P. Gomes, L. Visscher, H. Bolvin, T. Saue, S. Knecht, T. Fleig and E. Eliav, *The Journal of Chemical Physics*, 2010, **133**, 064305.

28 L. I. Grossweiner and M. S. Matheson, *The Journal of Physical Chemistry*, 1957, **61**, 1089–1095.

29 U. Banin, A. Bartana, S. Ruhman and R. Kosloff, *The Journal of Chemical Physics*, 1994, **101**, 8461–8481.

30 U. Banin, R. Kosloff and S. Ruhman, *Chemical Physics*, 1994, **183**, 289 – 307.

31 R. Nakanishi, N. Saitou, T. Ohno, S. Kowashi, S. Yabushita and T. Nagata, *The Journal of Chemical Physics*, 2007, **126**, 204311.

32 J. Vala, R. Kosloff and J. N. Harvey, *The Journal of Chemical Physics*, 2001, **114**, 7413–7423.

33 T. Migchelsen and A. Vos, *Acta Crystallographica*, **23**, 796–804.

34 C. J. Margulis and D. F. Coker, *The Journal of Chemical Physics*, 2000, **113**, 6113–6121.

35 P. Tasker, *Molecular Physics*, 1977, **33**, 511–518.

36 W. Gabes and M. A. M. Nijman-Meester, *Inorganic Chemistry*, 1973, **12**, 589–592.

37 G. C. Pimentel, *The Journal of Chemical Physics*, 1951, **19**, 446–448.

38 Y. T. Lee, P. R. LeBreton, J. D. McDonald and D. R. Herschbach, *The Journal of Chemical Physics*, 1969, **51**, 455–456.

39 A. D. Walsh, *Journal of the Chemical Society*, 1953, 2266–2288.

40 A. Viste and P. Pyykkö, *International Journal of Quantum Chemistry*, **25**, 223–231.

41 C. J. Margulis, D. A. Horner, S. Bonella and D. F. Coker, *The Journal of Physical Chemistry A*, 1999, **103**, 9552–9563.

42 C. J. Margulis and D. F. Coker, *The Journal of Chemical Physics*, 2001, **114**, 6744–6749.

43 A. L. Kaledin, M. C. Heaven, K. Morokuma and D. M. Neumark, *Chemical Physics Letters*, 1999, **306**, 48 – 52.

44 R. M. Jones and S. L. Anderson, *Review of Scientific Instruments*, 2000, **71**, 4335–4337.

45 E. Hendell and U. Even, *Review of Scientific Instruments*, 1995, **66**, 3901–3902.

46 R. E. Continetti, D. R. Cyr, D. L. Osborn, D. J. Leahy and D. M. Neumark, *The Journal of Chemical Physics*, 1993, **99**, 2616–2631.

47 J. M. B. Bakker, *Journal of Physics E: Scientific Instruments*, 1974, **7**, 364.

48 X. Xie and J. D. Simon, *Optics Communications*, 1989, **69**, 303 – 307.

49 K. A. Hanold, A. K. Luong, T. G. Clements and R. E. Continetti, *Review of Scientific Instruments*, 1999, **70**, 2268–2276.

50 D. P. de Bruijn and J. Los, *Review of Scientific Instruments*, 1982, **53**, 1020–1026.

51 K. A. Hanold, C. R. Sherwood and R. E. Continetti, *The Journal of Chemical Physics*, 1995, **103**, 9876–9879.

52 Q. Hu, H. Song, C. J. Johnson, J. Li, H. Guo and R. E. Continetti, *The Journal of Chemical Physics*, 2016, **144**, 244311.

53 A. T. J. B. Eppink and D. H. Parker, *Review of Scientific Instruments*, 1997, **68**, 3477–3484.

54 R. Li, K. A. Hanold, M. C. Garner, A. Khai Luong and R. E. Continetti, *Faraday Discussions*, 1997, **108**, 115–130.

Photoelectron-photofragment coincidence studies of I_3^- using an electrospray ionization source and a linear accelerator table of contents entry:
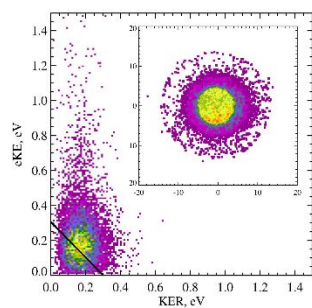
New insights into the dissociative photodetachment and the charge-symmetric three-body photodissociation of I_3^- are provided by photoelectron-photofragment coincidence spectroscopy.